Walraven.

Helium-temperature beam source of atomic hydrogen

J. T. M. Walraven and Isaac F. Silvera

Natuurkundig Laboratorium der Universiteit van Amsterdam, Valckenierstraat 65, 1018 XE Amsterdam, The Netherlands

(Received 13 July 1981; accepted for publication 23 April 1982)

We describe a technique for producing a high-flux beam of atomic hydrogen with a velocity distribution corresponding to liquid-helium temperatures. We have studied how a gas of hydrogen atoms (H) may be cooled to low temperatures through interaction with cold walls. The gas was analyzed by forming an atomic beam. We obtained fluxes $\phi_H \simeq 2.4\times10^{16}$ atoms/s at $T\simeq 8$ K, which corresponds to an increase in flux of low-velocity atoms by a factor of 20 over that of the same source operated at room temperature. The degree of dissociation and the translational temperature of the gas were determined using a quadrupole mass spectrometer and time-of-flight techniques. A beam modulation technique advantageous for such a system is discussed and analyzed. General design considerations for the transport and cooling of H are presented and illustrated with examples. The methods of data analyses are discussed in detail.

PACS numbers: 07.77. + p, 41.80. − y

INTRODUCTION

In this paper we discuss a method by which atomic hydrogen (H), produced at room temperature, is cooled to helium temperature through interaction with cold walls, providing a high-flux source. Although there exists extensive literature on sources of H, only very recently have there been any reports of sources of liquid helium temperature H.[1,2,3] The work described here has been motivated by our endeavors to produce a stable gas of atomic hydrogen at low temperature for studies of its predicted properties as a weakly interacting Bose gas.[4] However, the source is not limited to this type of research and should have potential applications in many areas. As a time and frequency standard the hydrogen maser can be improved by low-temperature operation.[5,6] Low velocity H beams are required to study the well region of the interaction potential of (for instance) the H + H_2 system.[7] Considerable interest also exists in high-energy physics where low-velocity atoms are of interest to improve the intensity of polarized proton sources and targets.[8-11]

The feasibility of cooling H to helium temperatures has been demonstrated in numerous experiments where gaseous mixtures of H, H_2, and (often) inert gases are rapidly condensed onto a cold substrate in order to matrix isolate the H atoms.[12,13] However, these experiments yield little information about the efficiency of the cooling process. The present work is aimed towards the study of the experimental conditions by which H can be cooled to low temperatures and the efficiency of this process with respect to recombination. Our experimental approach is to run H through a short cylindrical tube of variable temperature, the walls of which act as an accommodator. The gas emerging from the accommodator forms an atomic beam and is analyzed using standard beam techniques. In this way we determine the atomic flux, degree of dissociation, and translational temperature of the gas. The measurements also enable an estimate of the average density of H in the accommodator. Although the paper gives an account of these measurements, we have tried to emphasize design and measurement technique considerations, in particular the transport of a recombining gas of hydrogen. The advantages and use of an equal segmented chopper blade for time-of-flight measurements of hydrogen, rather than the usual narrow slit chopper, are discussed in detail. To our knowledge this technique has not been discussed in the literature.

We have divided this paper into three main sections. First (Sec. I) we discuss our experimental apparatus along with design considerations; Sec. II is devoted to the procedures employed in the measurements and the results are presented and discussed in Sec. III.

I. THE EXPERIMENTAL APPARATUS

A. Overview

A schematic diagram of the apparatus is given in Fig. 1. H is produced at the left in a water cooled fused-quartz discharge tube inserted into a microwave dissociator operated at 2450 MHz. The discharge pressure is adjusted in the range 0.5–1.5 Torr using a needle valve which also serves to limit the total flow through the system. Typically the dissociated fraction is 90%. The atoms flow through a small orifice into a Teflon tube which serves to guide the atoms toward a cylindrical accommodator (4 mm inner diameter, 20 mm long) intended to cool the H gas to liquid helium temperatures. For this purpose a small He cryostat with vapor cooled shielding is incorporated in the system. The beam emerging from the accommodator is differentially pumped in three stages to obtain pressures on the order of 10^{-9} Torr in the last stage, where a quadrupole mass spectrometer is used as a detector. The beam intensity is modulated in the second stage using an equal segmented chopper blade. The dis-

 0034-6748/82/081167-15$01.30

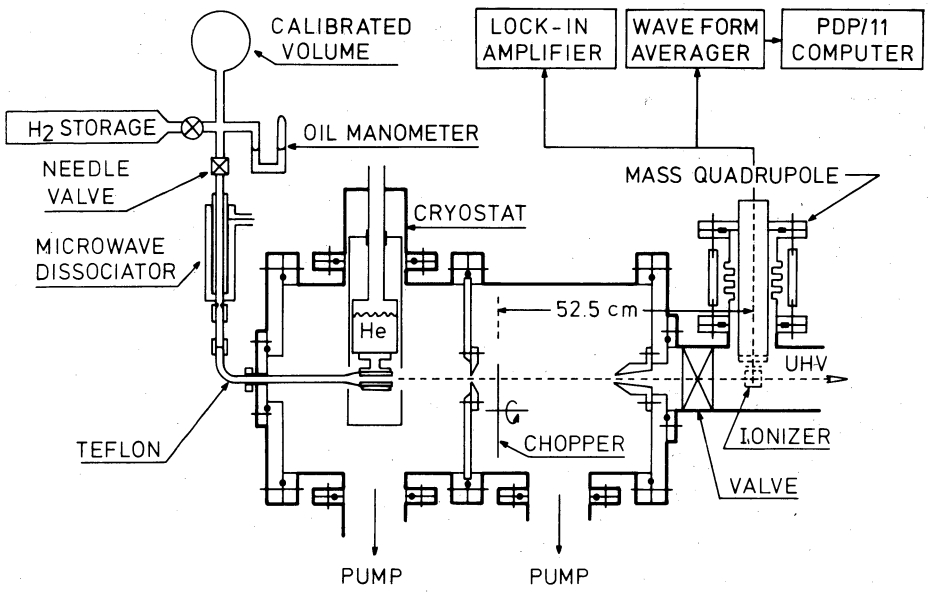

FIG. 1. Schematic drawing of the apparatus. Details of the dissociator, etc. are given in subsequent figures.

tance between chopper and detector (52.5 cm) enables a time-of-flight (TOF) analysis of the beam, using a waveform averager and a PDP/11 computer for signal processing. Since we use an equal segmented chopper blade, the velocity distributions are found by differentiation of the detector response. The principle advantage of this method is that one obtains a high average flux, which enables easy alignment and continual monitoring of the beam intensity with a lock-in amplifier. This is particularly important with a species such as H in which rapid beam deterioration can result in signal averaging of a nonexistent signal and much wasted effort. A boxcar integrator was used for absolute intensity measurements. For these measurements the gas handling system included a calibrated volume of 1140 cc and an oil manometer.

B. The dissociator

Many publications concerning dissociation of hydrogen have appeared in the literature, discussing the specific problems associated with various techniques.[14] Thermal beams of hydrogen atoms are currently produced using electrodeless discharges employing rf or microwave power. We use a homemade reentrant cavity operated at 2450 MHz (λ = 122 mm). The cavity, shown in Fig. 2, consists of a 28-mm i.d. outer conductor (OC) of length $5\lambda/4 \simeq 153$ mm and a (slightly shorter) inner conductor (IC) of 14.8 mm o.d. A quartz discharge tube is inserted coaxially through the IC and the discharge occurs in the gap of approximately 3.5 mm between the end of the IC and a cap tightly fitting over the end of the OC. The cavity is tuned capacitively by varying the gap spacing. For this purpose the IC can be moved relative to the OC using a fine adjustment screw. A simple $\lambda/4$ finger joint[15] was used to minimize electrical losses in the sliding contact. The power is coupled in inductively via an N-type connector making contact with the IC via the finger joint. The discharge is started using a spark from a tesla coil.

A variety of discharge tubes were tried. The discharge was most easily operated using a 12-mm o.d. quartz tube which completely filled the bore of the inner conductor; however, poor cooling inherent to this geometry caused a high operating temperature and resulted in irreversable deterioration of the tube after a few hours. Deteriorated tubes invariably showed a dark deposit, sometimes exhibiting a metallic appearance. The surfaces usually could be cleaned somewhat using a strong oxidizing acid mixture ($HNO_3 + H_2SO_4$). However, the only way to completely remove the dark film was to wash the tube in concentrated HF or NaOH for many hours after which the film "peeled off" but did not dissolve. Our chemical experiences are consistent with the Auger analysis of darkened surfaces of Pyrex dissociator envelopes obtained by Ritz *et al.*,[16] who attributed the films to deposits of carbon in its amorphous and carbide forms and to a lesser extent to Si_3N_4. Many procedures were tried to clean the tubes but in our experience the best way to improve the discharge in the case of deterioration was to replace the tube.

In our present system the discharge region is cooled from two sides, as shown in Fig. 3, using water as a coolant, carefully shielded from the microwave by a metal envelope. Additional cooling is obtained by blowing

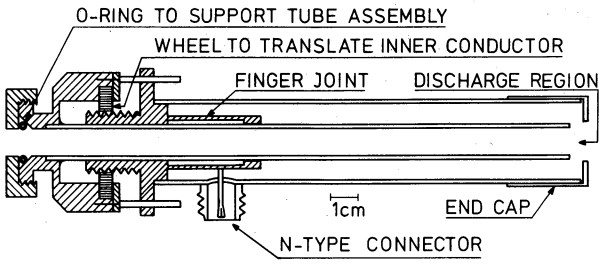

FIG. 2. Microwave cavity operating at 2450 MHz. The assembly of discharge tube and water cooling shown in Fig. 3 fits into the inner conductor. While the inner conductor remains fixed in position with respect to the discharge tube the outer conductor can be translated to tune the cavity for optimum coupling.

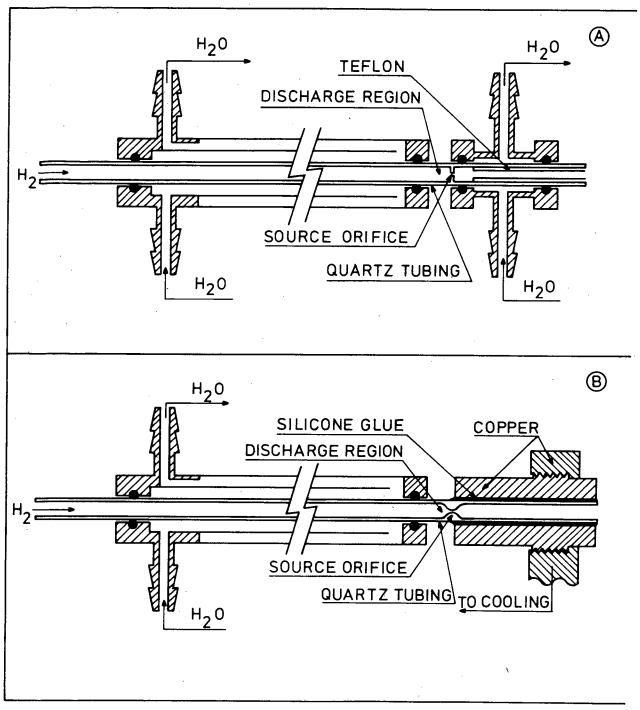

FIG. 3. Two examples of discharge-tube assemblies. (A) Water-cooled system used for room-temperature dissociation. (B) Assembly where the temperature of the outstreaming gas can be varied from 77 to 600 K by varying the temperature of a copper cold plate.

air in the gap region. Incorporation of the cooling facilities limited the size of the discharge tube to approximately 6 mm outer diameter and was found to make the tuning procedure a bit more subtile. Typically the dissociator is operated at a pressure of 0.5 Torr using 25 W of microwave power; the system reliably yields a degree of dissociation on the order of 90% up to a few torr. We use standard 6 × 4-mm quartz tubing in which a flow impedance is fused in to separate the discharge region from the transport tube which serves to guide the atoms to the accommodator. The impedance is a 0.35-mm orifice in a disk of 1 mm thickness sliced off from thick-walled quartz capillary tubing. Connections to the discharge tube are made using standard Teflon swagelock vacuum connectors.

C. Transport of the gas

A flexible Teflon tube connects the dissociator with the accommodator. We shall present a simple phenomenological model describing Knudsen flow of atoms through the tube in the presence of surface recombination. The model enables an estimate of the recombination losses. For convenience the last two centimeters of the tube are supposed to represent the accommodator and will be considered to be at the same temperature as the tube for our present purpose. The model is very useful for design purposes, where often only an estimate of the effect of recombination is required. More accurate results can be obtained with an analysis in terms of exact integral equations.[17,18] The viscous flow regime is reviewed by Wise and Wood.[19] A useful formulation of the problem, in view of our needs, is obtained by considering a tube of length l and radius r closed at the left and open at the right end and maintained at room temperature. The tube is assumed to be "long" ($l \gg r$). At the left-hand side we introduce H through a small orifice at the rate ϕ_{in}; the other side is assumed to end in an ideal vacuum. In the case of Knudsen flow we may estimate the density profile of H along the tube as well as the degree of dissociation of the gas leaving the tube using a diffusion model

$$\phi(z) = -\pi r^2 D_{Kn} \frac{dn(z)}{dz}, \tag{1}$$

where $\phi(z)$ and $n(z)$ represent the atomic flux and density at distance z in the tube measured from the high-pressure end, $D_{Kn} \equiv \frac{2}{3} r\bar{v}$ is the atomic diffusion constant for Knudsen flow, and $\bar{v}$ is the average atomic velocity. The variation of $\phi(z)$ along the tube due to recombination is written phenomenologically as a power series in $n(z)$:

$$\frac{d\phi}{dz} = -\pi r^2 K_v n^3 - 2\pi r K_{S2} n^2 - 2\pi r K_{S1} n. \tag{2}$$

the first term describes three-body volume recombination, with rate constant K_v, the two other terms arise from surface recombination which can be first or second order in nature, with rate constants K_{S1} and K_{S2}.[20] The surface density σ is built up of two components: $\sigma = \sigma_t + \sigma_m$. σ_t is the density of atoms trapped in catalytic sites. Below an activation temperature (which may be much higher than room temperature) these sites will be continuously saturated and σ_t will be a constant equal to the density of these sites. The second component, σ_m, represents weakly bound (physisorbed) mobile atoms. σ_m and σ_t are related to the bulk gas density through an adsorption isotherm. σ_m is proportional to n in the limit of low coverages. Recombination may proceed through interactions of trapped atoms with mobile surface atoms or with gas-phase atoms, giving rise to first order recombination, or between two mobile adsorbate atoms resulting in second order recombination. On Pyrex and quartz, recombination is known[19] to be first order over a wide range of temperatures, however, for $T \lesssim 120$ K and $T \gtrsim 550$ K, recombination is a second-order process. At room temperature, recombination on Teflon is thought to be first order[21] and we shall assume this to be the case.

Using Eqs. (1) and (2) the diffusion problem is reformulated for Knudsen flow as

$$\frac{d^2n}{dz^2} = \frac{3}{r^2\bar{v}}\left(K_{S1} n + K_{S2} n^2 + \frac{1}{2} r K_v n^3\right) \tag{3a}$$

$$\frac{dn}{dz} = \frac{1}{2\pi}\frac{3}{r^3\bar{v}}\phi \tag{3b}$$

with boundary conditions $n(z = l) = 0$ and $\phi(z = 0) = \phi_{in}$. For our present purpose volume recombination will be shown to be negligible so that we limit the analysis to surface recombination. In the absence of any recombination ($\phi_{out} = \phi_{in}$) we obtain the well known relations for Knudsen flow[22]:

$$n(z) = n_0(1 - z/l) \tag{4}$$

$$n_0 = \frac{3}{2\pi}\frac{l}{r^3\bar{v}}\phi_{in}\,. \tag{5}$$

Equation (5) is often written in the Clausing form[23]

$$\phi_{out} = \tfrac{1}{4}Kn_0\bar{v}A, \tag{6}$$

where $A = \pi r^2$ is the cross section of the tube and $K = \frac{8}{3}(r/l)$ is the Clausing factor in the Knudsen limit (long tubes). For short tubes values for K are tabulated.[24] The average number of wall collisions, $\bar{N}_c$, that a particle has undergone after diffusing through the tube is given by

$$\bar{N}_c = \frac{\phi_{wall}}{\phi_{out}} = \frac{3}{8}\left(\frac{l}{r}\right)^2, \tag{7a}$$

where $\phi_{wall} = \int_0^l \tfrac{1}{4}n(z)\bar{v}2\pi r\,dz$ is the total number of wall collisions per unit time. The average time the particle has spent in the tube is given by

$$\bar{t} = \frac{N_{tot}}{\phi_{out}} = \frac{3}{4}\frac{l^2}{r\bar{v}}\,. \tag{7b}$$

Here $N_{tot} = \int_0^l n(z)\pi r^2\,dz$ is the total number of atoms in the tube. We note that in general ϕ_{wall} and N_{tot} include a contribution due to particles which never reach the end of the tube. This is, for instance, the case in the classical geometry of Knudsen (a channel connecting two big vessels), where only a fraction z/l of the particles colliding with the wall at a distance z in the tube will reach the end. The rest of the particles return to the primary vessel. As a result, only a third of the particles in the channel will reach the secondary end, in which case

$$\bar{N}_c = \frac{1}{8}\left(\frac{l}{r}\right)^2 \quad \text{and} \quad \bar{t} = \frac{1}{4}\frac{l^2}{r\bar{v}}\,. \tag{8}$$

Our geometry is characterized by a negligible probability to return to the discharge region ($\phi_{in} = \phi_{out}$) and thus Eqs. (7a) and (7b) are applicable.

In the case of first-order recombination the rate coefficient can be written as $K_{S1} \equiv \tfrac{1}{4}\gamma\bar{v}$, where γ is the recombination probability per wall collision. With this convention the solution of Eqs. (3a) and (3b) is

$$n(z) = \frac{n_0}{\sqrt{2\gamma\bar{N}_c}}\frac{\sinh[\sqrt{2\gamma\bar{N}_c}(1 - z/l)]}{\cosh[\sqrt{2\gamma\bar{N}_c}]}\,. \tag{9a}$$

$\bar{N}_c$ is given by Eq. (7a). n_0 is the atomic density, achieved immediately behind the source orifice and calculated using Eq. (5). A plot of $n(z)$ vs z is given in Fig. 4. The degree of dissociation, α, of the flux leaving the tube, defined as the fraction of all atoms in the dissociated state [$\alpha \equiv n_H/(n_H + 2n_{H_2})$] may be expressed [using Eq. (3b)] as

$$\alpha \equiv \frac{\phi(l)}{\phi_{in}} = [\cosh\sqrt{2\gamma\bar{N}_c}]^{-1}. \tag{9b}$$

We note that the actual purity of the gas is higher (dissociation of one molecule yields two atoms) but in conforming with the literature on dissociation we shall use

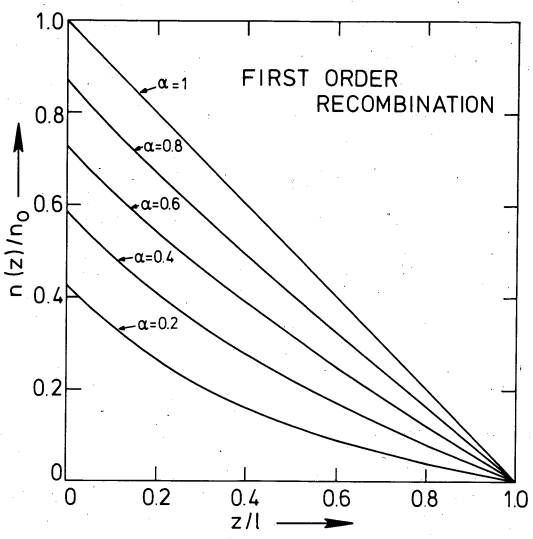

FIG. 4. Density profile of atomic hydrogen along a tube with length l for the case of first-order recombination. α is the degree of dissociation of the gas leaving the tube.

α. Furthermore, $\alpha \simeq 0.46$ for $\gamma\bar{N}_c = 1$ so that, as a rule of thumb, for negligible recombination in the tube one should require

$$\gamma\bar{N}_c \ll 1. \tag{9c}$$

Our objective is to use these results for designing a source with an acceptable output flux. As an example we consider the Teflon tube of typical length $l = 25$ cm and radius $r = 2.5$ mm. We first estimate ϕ_{in}. In the discharge, operated at 0.5 Torr, the atomic density is estimated to be $n_d \simeq 8 \times 10^{15}$/cc (for 600 K and full dissociation). This implies $\phi_{in} \simeq \tfrac{1}{4}K_0n_d\bar{v}A_0 \simeq 1.8 \times 10^{17}$/s for the flux entering the transport tube, where $K_0 \simeq 0.25$ is the Clausing factor and $A_0 \simeq 0.1$ mm^2 is the area of the source orifice. We calculate $n_0 \simeq 6 \times 10^{14}$/cm^3 using Eq. (5), corresponding to a mean free path[25] of a few millimeters so that Knudsen flow may be assumed. Volume recombination can be neglected if $\tfrac{1}{2}rK_vn^3 \ll K_{S1}n$. This requirement leads to an upper limit for the density:

$$n \ll \left(\frac{\gamma\bar{v}}{2rK_v}\right)^{1/2}. \tag{10}$$

Using the data of Mitchell and Le Roy[21] ($\gamma_{Teflon} = 2.1 \times 10^{-5}$ and $K_v \simeq 1.2 \times 10^{-32}$ cm^6 atom^{-2} s^{-1}) we conclude $n \ll 3 \times 10^{16}$/cm^3, a condition easily met without limiting n_0.

The degree of dissociation at the end of the tube can now be evaluated with the aid of Eq. (9b). We find $\alpha \simeq 93\%$. However, if we were dealing with an imperfect Teflon *coating* on a Pyrex tube and 5% of the Pyrex was exposed to the atoms, we would have a larger effective recombination coefficient ($\gamma_{eff} \simeq 2.2 \times 10^{-4}$, with $\gamma_{Pyrex} \simeq 4 \times 10^{-3}$, see Ref. 19) yielding $\alpha \simeq 51\%$. This example shows that Teflon tubing can be used to guide H atoms over relatively large distances without excessive recombination and that Pyrex is inadequate for this purpose, at least at room temperature. For a similar uncoated Pyrex tube one finds $\alpha \simeq 8 \times 10^{-3}$. However, cooling this

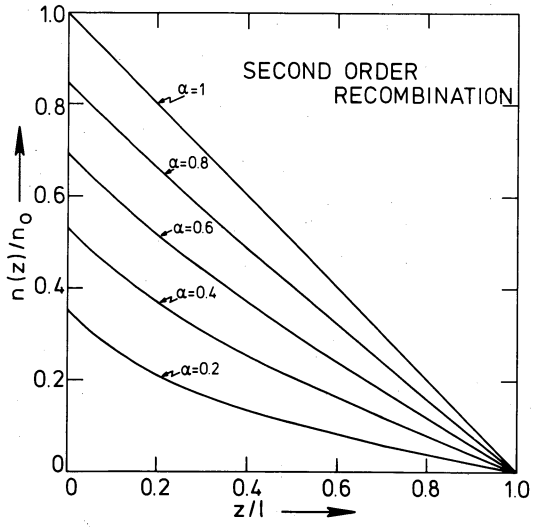

FIG. 5. Density profile of atomic hydrogen along a tube with length l for the case of second-order recombination. α is the degree of dissociation of the gas leaving the tube.

tube to ~100 K, where the recombination coefficient for Pyrex is minimal, one again finds $\alpha \simeq 93\%$, since for this temperature $\gamma_{\text{Pyrex}} \simeq \gamma_{\text{Teflon}} \simeq 2 \times 10^{-5}$. One should notice that recombination coefficients may vary from sample to sample as witnessed by the large scatter in γ_{Pyrex} values[26–29] obtained by various authors in the literature. We have observed a Teflon surface to deteriorate "overnight" in a vacuum chamber, probably due to oil contamination.

In view of these uncertainties the calculated values for α agree fairly well with the experimental results, where values of α up to ≃60% were obtained using commercial Teflon tubing for the transport tube and Teflon coated quartz tube of 4 mm inner diameter for the accommodator and for the first section of the tube, i.e., the section immediately behind the discharge region (see Fig. 1). A very pure atomic beam ($\alpha > 90\%$) was obtained using a 90-mm-long × 4-mm-wide uncoated quartz tube operated at nitrogen temperature (see Fig. 3b).

For second-order recombination the probability of recombination per wall collision becomes density dependent ($\gamma \equiv 4K_{S2}n/\bar{v}$). If we still use this concept to express our results the solution of Eqs. (3a) and (3b) is given by

$$n(z) = \frac{n_0}{\gamma_0 \bar{N}_c (a + z/l)} x^2 P(x; 0, 1), \tag{11a}$$

$$\alpha \equiv \frac{\sqrt{-\xi}}{\gamma_0 \bar{N}_c a^3}, \tag{11b}$$

where $P(x; 0, 1)$ is the equianharmonic case of the Weierstrass elliptic function[30] and $\gamma_0 \equiv \gamma(z = 0)$. Furthermore,

$$x(z) \equiv \left(\frac{2\omega_2}{\sqrt{3}}\right)\left(\frac{(z/l + a)}{(1 + a)} e^{i(\pi/6)}\right) \tag{11c}$$

$x_0 \equiv x(z = 0)$, $\xi = x_0^6$ and $\omega_2 \simeq 1.53$ (see Ref. 30). The constant a has to be determined from the relation

$$\gamma_0 \bar{N}_c = -\left(\frac{x_0}{a}\right)^3 P'(x_0; 0, 1). \tag{11d}$$

A plot of $n(z)$ vs z according to Eq. (11a) is given in Fig. 5 for various values of α.

Equations (11a) and (11d) are most conveniently manipulated using economized polynomial expansions for $x^2P(x; 0, 1)$ and $x_0^3P'(x_0; 0, 1)$.[31] In terms of these polynomials $n(z)$ is given by

$$n(z) = \left(n_0 \frac{a^3}{(z/l + a)}\right)\left(\frac{P_1(\eta)}{P_2(\xi)}\right). \tag{12a}$$

The constant a (or ξ) has to be determined from

$$\gamma_0 \bar{N}_c = -\frac{P_2(\xi)}{a^3}. \tag{12b}$$

To a good approximation [for $0 \le \eta$ (or ξ) ≤ 12.8]

$$P_1(\eta) = 1 + 3.571 \times 10^{-2}\eta + 9.8 \times 10^{-5}\eta^2 \tag{12c}$$

$$P_2(\xi) = -2 + 0.14286\xi + 9.81 \times 10^{-4}\xi^2. \tag{12d}$$

Here $\eta \equiv x^6$.

The case of second-order recombination is illustrated with the example of a tube with the same dimensions as the Teflon tube discussed earlier (l = 25 cm and r = 2.5 mm) but now maintained at T = 0.5 K and covered with a superfluid film of ^{4}He. Assuming a flux $\phi_{\text{in}} = 8 \times 10^{15}$/s to enter the tube via a small orifice we again calculate $n_0 \simeq 6 \times 10^{14}/\text{cm}^3$ using Eq. (5) so that the assumption of Knudsen flow is justified.[32] Volume recombination may be neglected if $n \ll \frac{2K_{S2}}{rK_v}$ as seen from Eq. (3a). Using the data of Morrow *et al.*,[6] $K_{S2} = 8 \times 10^{-17}$ cm^4/s, for T = 0.5 K and $K_v = 2.8 \times 10^{-33}$ cm^6/s as measured by Hardy *et al.*,[33] we find $n \ll 2.3 \times 10^{17}/\text{cm}^3$. This condition is easily satisfied over the whole length of the tube. Using $\gamma \equiv 4K_{S2}n/\bar{v}$, (7a), (12b) and (11b), we may calculate $\gamma_0 \bar{N}_c \simeq 0.14$, $a \simeq 2.65$, $\xi = -4.45$ and $\alpha = 0.81$. At this low temperature α does not represent the degree of dissociation (which is unity since H_2 will freeze out on the walls) but simply the reduction in flux due to recombination. We note that under these conditions transport of atoms at 0.5 K is comparable in efficiency with transport at room temperature with a Teflon tube. However, in a high magnetic field recombination is known to be strongly suppressed at low temperatures. Matthey *et al.*,[34] measured $K_{S2} \simeq 3.8 \times 10^{-21}$ cm^4/s in 10 T at T = 0.5 K. With this figure we calculate for a tube of l = 2500 cm and r = 2.5 mm $\gamma_0 \bar{N}_c = 0.068$, again using $n_0 = 6 \times 10^{14}/\text{cm}^3$ (or $\phi_{\text{in}} \simeq 8 \times 10^{13}$/s). Thus, a = 3.50, $\xi = -6.73$ and $\phi_{\text{out}} = 0.89\ \phi_{\text{in}}$. We note that the atoms have spent on the average a time of 1875 s in the tube, as determined by Eq. (7b), without significantly recombining. These results may be extended to other temperatures or other magnetic fields ($B > 0.5$ T) using $K_{S2} = K_0 B^{-2} T^{-1/2} \exp(2\epsilon_a/kT)$,[34] where K_0 is a scaling constant and ϵa the surface adsorption energy.

D. The accommodator

The considerations of the preceding section can also be used for the design of an efficient accommodator. The

aim is to cool the fluxing gas down to approximately the temperature of the surface without it recombining. At 4.2 K, the best known accommodator surface, with a low vapor pressure, is H_2. However, we point out that H_2 has an adsorption energy $\epsilon_a/k = 38 \pm 5$ K for H.[35] In thermodynamic equilibrium most of the H would rapidly condense and recombine. Thus, the accommodator design must be such that the gas just approaches the wall temperature and then fluxes out into a subsequent stage. Accommodation can usually be achieved with just a few collisions so that a choice of $\bar{N}_c \simeq 1/\gamma$, resulting in $\alpha \simeq 50\%$, [see relation (9c)] is satisfactory.

From these qualitative arguments one concludes that one should select wall materials with small adsorption energy, ϵ_a, for use at low temperatures. Then the surface coverage and thus γ will remain minimal. The best known surfaces to inhibit condensation of H are made of liquid ^{4}He, ^{3}He, or ^{3}He–^{4}He mixtures with a measured $\epsilon_a \simeq 0.9$ and 0.34 K, respectively.[6,34,36,37] However, use of these surfaces require very low temperatures to maintain a low density of the saturated helium vapor which catalyzes volume recombination. Therefore, except for the lowest temperature ($T \lesssim 0.6$ K) one must rely on other surfaces with a weak physisorption potential for H, such as H_2 or Ne. From the work of Crampton[35] we calculate $K_{S2} \simeq 3 \times 10^{-12}$ cm^4/s at $T = 4.2$ K. With the aid of $\gamma \equiv (4/\bar{v})K_{S2}n$ and using $n = 10^{13}$/cm^3 one finds $1/\gamma \simeq 250$ showing that only very short H_2 plated tubes can be used to accommodate H to 4.2 K.

In practice it is difficult to select a well characterized geometry to cool H. Surface composition is often poorly known and temperature gradients complicate the picture; therefore, we have tested several accommodator designs. Initially we followed the concept utilized by Toennies, Welz, and Wolf (TWW),[7] first described by Wilsch.[38] In this design H, produced by rf discharge, is cooled to ~90 K by passing the gas through a narrow metal channel cooled with liquid nitrogen. Various wall materials were tested by TWW (Pyrex, boron nitride, copper), but best results were obtained using an aluminum channel. Since aluminum surfaces efficiently catalyze surface recombination,[19] the result was attributed to the formation of a thin oxide layer efficiently cooled by the metallic substrate. It is interesting to note that we have observed the *copper*-oxide surface to be unstable in direct contact with H. A black, heavily oxidized, copper sample regained its metallic appearance in a few minutes under bombardment with H at a rate of 10^{17}/cm^2 s. TWW also tried cooling their beams to hydrogen temperature (20.4 K), however, under these conditions considerable recombination took place while the remaining atoms were not effectively accommodated.

Following the concept of TWW an aluminum cap, containing a 0.5-mm-diam channel, was attached to the (uncooled) end of our discharge tube. We found a good thermal contact between the aluminum and quartz to be of vital importance to prevent the discharge tube from overheating. This requirement caused a considerable heat load on the cooling system. Although the degree of dissociation was high (>90%) down to nitrogen temperature, cooling to helium temperatures was unsuccessful, while the system was susceptible to breakage due to differential thermal contraction.

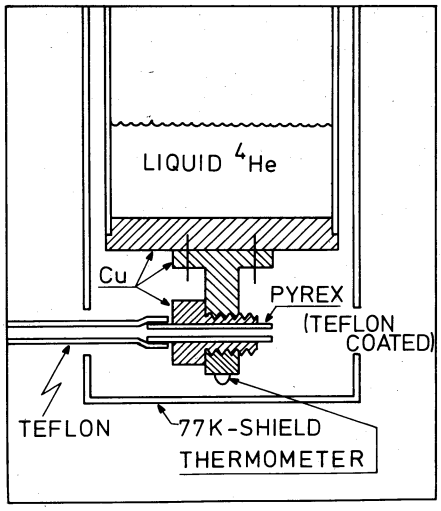

FIG. 6. Schematic diagram of the low-temperature section of a helium cryostat used to cool a Teflon coated Pyrex tube to helium temperatures.

Good dissociation was also obtained using a discharge tube as drawn in Fig. 3(b). This tube was partially water cooled and partially cooled with liquid nitrogen. For this purpose the quartz tube was glued into a copper cylinder using silicone cement, and an adhesive remaining reasonably flexible at low temperature and consequently capable of compensating for the rather large differences in thermal contraction between copper and quartz. The copper cylinder was screwed into an aluminum cold plate cooled by circulation of cryogenic liquids. Although this geometry worked very reliably down to liquid nitrogen temperature, it had the disadvantage that a considerable fraction of the microwave power dissipated in the discharge still had to be carried away through the low-temperature cooling system, limiting the lowest achievable temperatures to about 20 K.

The most detailed study was made using a design where the accommodator is completely thermally decoupled from the discharge region (see Fig. 1). The atoms are guided to the accommodator using Teflon tubing. In this way an extremely flexible geometry is obtained. For an accommodator we used a cylindrical Pyrex tube (6 × 4 mm; 20 mm long) coated with Teflon, using FEP Teflon dispersion[39] fused at 350 K in a flowing oxygen atmosphere. Using Eq. (7a) we calculate $\bar{N}_c \simeq 38$. The accommodator was glued into a copper block, again employing silicone glue. The block is screwed to the bottom of a small can which holds approximately 1 l of liquid helium. The arrangement is shown in Fig. 6. The main disadvantage of this design was that for high flows a background gas built up interfering with the beam and thus limiting the fluxes that could be studied. The properties of the accommodator were studied as a function of temperature. At high temperature the Teflon surface is exposed to the H gas, whereas at helium temperature

the Teflon is coated by H_2. The lowest achievable temperatures were limited to 7.7 K due to conduction and radiative heat leaks. For an accommodator used in studying H as a stable low-temperature gas,[4] we simply used a copper or german silver wall which is coated with H_2 at $T \simeq 5$ K.

E. Beam formation

The atomic beam that results when the gas leaving the accommodator expands into a vacuum can be described by a model of Giordmaine and Wang (GW),[40] who successfully applied kinetic theory to the problem of molecular beam formation by long cylindrical channels connecting a source volume to an ideal vacuum. A similar study was made by Troitskii.[41] GW assumed the density $n(z)$ to fall linearly with the distance (z) along the channel as in the case of Knudsen flow

$$n(z) = n_s(z/l), \tag{13}$$

where n_s is the density in the source, z is measured from the low-pressure end, and l is the total length of the channel. Better approximations accounting for the nonzero density at the end of a real channel have also been studied[42] but lead to corrections which hardly affect our results.

GW considered two contributions to the center-line intensity, I, of the beam: (a) A contribution due to atoms passing through the channel without collisions

$$I_1 = \frac{1}{4\pi} n_s \bar{v}_s A \exp\left(\frac{-l}{2\lambda s}\right), \tag{14}$$

where λ_s is the molecular mean free path at density n_s and the exponent accounts for beam attenuation due to scattering by the stagnant gas in the channel. (b) A contribution due to particles scattered into the axial direction by interatomic collisions in the channel.

$$I_2 = \int_0^l dz \frac{1}{4\pi} n(z)\bar{v}A \frac{1}{\lambda(z)} \exp\left(\frac{-z}{2\lambda(z)}\right). \tag{15}$$

Adding Eqs. (14) and (15) one attains the total center-line intensity which may be conveniently written as:

$$I = \frac{F(\eta)}{\pi} \frac{1}{4} n_s \bar{v} A \tag{16a}$$

$$F(\eta) \equiv \frac{\sqrt{\pi}}{2} \frac{\operatorname{erf}(\sqrt{\eta})}{\sqrt{\eta}} \tag{16b}$$

$$\eta \equiv l/2\lambda_s . \tag{16c}$$

F. Peaking of the beam

It will turn out to be useful to characterize a beam source with a parameter χ, called the peaking factor of the source, which relates the total intensity with the center-line intensity

$$I = \chi\Phi/\pi. \tag{17}$$

For a cosine emitting source $\chi = 1$ so that the peaking factor is a measure for the directivity of a beam source, normalized to that of an ideal effusive source. Comparing Eqs. (16) and (17), and recalling the well-known Clausing formula Eq. (6) for the total flow through a channel ($\Phi = \frac{1}{4}K_0 n_s \bar{v} A$; where K_0 is the Clausing factor) χ may be written as

$$\chi = F(\eta)/K_0 . \tag{18}$$

G. The opaque mode

A specific mode of operation, of particular importance for our analysis, is the opaque mode, where particles have a negligible probability to pass through the channel without a collision. In this mode we are still dealing with Knudsen flow but only process "b" will contribute to the beam. The condition for opacity in the channel is $\eta \gtrsim 6$, where the error function approaches unity to within 1% and can be approximated by

$$F(\eta) = \frac{1}{2}\left(\frac{\pi}{\eta}\right)^{1/2}. \tag{19}$$

Expressing λ in terms of the density, $\lambda = (\sqrt{2}\sigma n)^{-1}$, where σ is a collision cross section, and using the "long-channel approximation" for the Clausing factor [$K_0 = \frac{8}{3}(r/l)$] leads, after a few manipulations, to a compact formula for χ:

$$\chi = \frac{1}{8}\left(\frac{3}{2}\pi\sqrt{2}\frac{\bar{v}A}{r}\frac{1}{\Phi}\right)^{1/2}. \tag{20}$$

Equation (20) expresses a characteristic property of the opaque mode: for a given total flow the peaking factor is independent of the length of the channel.

H. Velocity distribution

Another property of importance for this study is the velocity distribution characterizing the channel sources. We assume thermal equilibrium in the source. Hence, the velocity distribution of the stagnant gas is given by the Maxwell–Boltzmann (MB) expression:

$$f_s(x)dx = 4\pi^{-1/2}x^2e^{-x^2}\,dx \tag{21a}$$

with normalization $\int_0^l f_s(x)dx = 1$ and

$$x \equiv \frac{v}{v_\alpha}; \quad v_\alpha \equiv (2kT/m)^{1/2}, \tag{21b}$$

where T is the source temperature, m the molecular mass, and k the Boltzmann constant. At pressures low enough that only process "a" will contribute to the beam (this is called the transparent mode of the channel source), one is clearly sampling the source volume in an "effusive" way, and the beam resulting from the channel possesses a velocity-weighted Maxwellian distribution[43]:

$$f_b(x)dx = 2x^3e^{-x^2}\,dx \tag{22}$$

again normalized to unity. If the source pressure is increased, the beam will be attenuated in the channel. In the GW-model this is accounted for by the exponentials in Eqs. (14) and (15).

In order to obtain a first-order correction to the velocity distribution, Olander, Jones, and Siekhaus (OJS)[44] extended the GW analyses, which is essentially a one-speed model, to allow for velocity dependence of the mean free path, utilizing the classical expression for the velocity averaged mean free path of a Maxwellian gas.[45] This model leads to a shift of the most probable velocity to a slightly higher value and predicts this effect to "saturate" with increasing opacity. In the opaque mode the velocity distribution is found to be independent of the total flow. OJS also reconsidered the peaking effect employing a velocity dependent mean free path, but the differences with the GW model were found to be insignificant for practical use and hence Eq. (20) remains adequate to estimate the peaking in channel sources.

Velocity distribution channel sources have been reported at various places in the literature.[46-48] However, none of these experiments showed the saturation effect in the opaque mode. To our knowledge, no adequate theory is available describing this aspect of the velocity distribution of channel sources.

II. MEASUREMENT PROCEDURES

A. Mass flow

The gas supply to the dissociator is controlled with a needle valve which determines the total flow through the system. The primary side of the valve is connected to a gas handling manifold, including branches to a simple oil manometer and a Pyrex bulb with a calibrated volume of 1140 cc. The bulb serves as an H_2 reservoir of known volume. Monitoring the pressure decay in the bulb as a function of time, by means of the oil manometer, enables an accurate determination of the mass flow (ϕ_m) through the system, defined as the flow of pairs of atoms (either in the atomic or molecular form). The data were corrected for dead volume in the gas handling system and for changes in the dead volume arising from varying levels in the oil manometer. During the measurements the temperature of the bulb was observed to be stable within 0.1 K. The reference arm of the manometer was continuously diffusion pumped to avoid errors caused by degassing of the oil. Typically our beams were operated at $\phi_m = 10^{17}$ pairs/s.

B. Calibration of the quadrupole for H_2

The quadrupole mass spectrometer is used to provide a convenient secondary standard for the mass flow through the system. Calibration is, however, not straight forward since the experimental arrangement, shown in Fig. 1, provides information only about the center-line intensity of the beam (I; units of the flux/sr) and not about the total flux (ϕ). As a result the peaking effects, discussed earlier, will complicate the analysis. Furthermore, the quadrupole measures the effective beam density in the ionizer, i.e., a velocity weighted intensity S instead of I directly:

$$S = \Gamma_0 (I/\bar{v}_s)\Omega L, \tag{23}$$

where Γ_0 is the ionization and extraction rate per particle, Ω is the solid angle of detection, L the length of the ionizer, and $\bar{v}_s = (8kT/\pi m)^{1/2}$, the average velocity in the source. In the case of non-Maxwellian velocity distributions, not $\bar{v}_s$, but (in general) a different weighting factor, is obtained. Γ_0 is in general a function of velocity as discussed by Siekhaus, Jones, and Olander.[46] This effect is strongly dependent on the type of ionizer and assumed to be negligible in our case since Maxwellian distributions were obtained for low source pressures. Combining Eqs. (17) and (23) yields

$$\phi = \frac{\pi}{\Omega L \Gamma_0} \frac{\bar{v}_s}{\chi} S. \tag{24}$$

With these considerations in mind an H_2 calibration of the quadrupole is obtained by chopping the beam with an equal segmented chopper and measuring the peak-to-peak value ($S_{\text{p.p.}}$) of the observed waveform with the quadrupole tuned to mass 2. $S_{\text{p.p.}}$ is proportional to the total H_2 flux as long as the period of the chopper function is much longer than the average time of flight through the system. A simultaneous measurement of ϕ_m, using the mass-flow technique discussed in the preceding section, provides the corresponding total flow ϕ_{H_2}, since for a purely molecular beam $\phi_{H_2} \equiv \phi_m$.

Once ϕ_m and $S_{\text{p.p.}}$ are determined for one specific combination of temperature and mass flow, scaling of χ and $\bar{v}_s$ may be used to obtain a calibration of the quadrupole reading for different temperature and flow conditions. Special care is required if the velocity distributions show deviations from Maxwellian behavior as a consequence of different velocity weighting in relation (24). Scaling of $\bar{v}_s$ is straightforward; scaling of χ is discussed later in this section.

C. Calibration of the quadrupole for H

The calibration procedure used for H_2 could also be applied to H if striking of the discharge in the dissociator would result in a 100% pure atomic beam, for then every molecule contributing to the mass flow (ϕ_m) through the flow impedance would simply result in a pair of atoms, or $\phi_H = 2\phi_m$. However, under typical experimental conditions the dissociation is not complete. The correction is straightforward once the degree of dissociation (α), i.e., the dissociated fraction of ϕ_m is known:

$$\phi_H = 2\alpha\phi_m . \tag{25}$$

D. The degree of dissociation

The experimental arrangement also enables a particularly simple determination of the dissociated fraction (α) of the beam by observation of the relative change in mass 2 intensity upon striking the discharge. First the H_2 signal (S_{pp}^{off}) is measured with discharge off. This provides us with a measure for the total H_2 flux, using Eq. (24), which equals the mass flux in this case. Then

the discharge is started and the H_2 signal drops until (after some transient effects) a new steady value is achieved (S_{pp}^{on}). Since the total mass flow is not affected by the status of the dissociator, the H_2 flux now represents a direct measure of the nondissociated fraction $(1-\alpha)$ of the mass flow:

$$(1-\alpha) = \phi_{H_2}^{on}/\phi_{H_2}^{off} = \frac{\chi_{off}\bar{v}_{on}S_{on}}{\chi_{on}\bar{v}_{off}S_{off}}. \tag{26}$$

By stabilizing the accommodator temperature one achieves $\bar{v}_{on} = \bar{v}_{off}$. This was checked experimentally by measuring the TOF distribution of H_2 with discharge on and discharge off. In practice, determinations of α were made using

$$\alpha \simeq 1 - \frac{S_{pp}^{on}}{S_{on}^{off}}. \tag{27}$$

This implies that errors due to possible changes of χ were neglected.

E. The density in the accommodator

An estimate for the (average) density in the accommodator is obtained in a simple way using Eq. (3b):

$$\bar{n} = \frac{3}{4\pi}\frac{l}{r^3\bar{v}}\phi. \tag{28}$$

Here l is the length of the accommodator and $\bar{v}$ is the average velocity of the stagnant gas. We note that this expression is only valid when the accommodator is operated in the opaque mode.

F. The peaking correction

The geometry of our system, as described in Sec. II deviates in various ways from the geometry studied by Giordmaine and Wang (GW). Nevertheless we shall assume the GW results to be transferable to our geometry as long as the source is operated in the opaque mode. This approximation can be considered to be a generalization of the result of Eq. (20) in the sense that it assumes the beam shape to be determined by the last section of the channel *only*. This section is defined by the condition $z \lesssim 2\lambda(z)$, where z is the distance in the accommodator, measured from the low-pressure end. This is the distance up to the point where the source becomes opaque. Furthermore, we require a homogeneous temperature distribution over the accommodator.

The concept of beam peaking as discussed before implies a change in peaking when the temperature of the accommodator is changed. This aspect of the theory is of particular importance for the calibration of our measurements. In a hard sphere collision approximation $\chi(T) \sim T^{1/4}$ as results from Eq. (20). The main uncertainty in $\chi(T)$ is due to the temperature dependence of σ, which was neglected in our estimates for the total atomic flux.

G. Time-of-flight analysis

Information about the temperature at which H leaves the accommodator can be obtained by pulsing the beam and using the quadrupole to observe the temporal dispersion of the pulses. We first present a somewhat general approach to be used in our subsequent analysis. If the shape of the pulse in time is represented by $e(t)$ the response of the detection system can be written as

$$S(t) = \underline{\underline{T}}e(t), \tag{29}$$

where $\underline{\underline{T}}$ is a linear operator. Let $h(t-t_0)$ be the linear response of the system to a δ-function pulse at $t = t_0$:

$$h(t-t_0) = \underline{\underline{T}}\delta(t-t_0) \tag{30}$$

with

$$\int_{-\infty}^{+\infty} h(t-t_0)dt = 1; \quad h(t-t_0) \equiv 0 \quad \text{for} \quad t < t_0 \text{ (causality)}. \tag{31}$$

The relation between the number of particles in the velocity interval $(v, v+dv)$ and the corresponding time interval $(t, t+dt)$ is

$$h_0(t-t_0) = -f_b(v)\frac{dv}{dt}, \tag{32}$$

where $t - t_0 \equiv L/v$, L being the distance between chopper and detector and h_0 is the real (i.e., uncorrected for detector properties) time-of-flight (TOF) distribution.

For a Maxwellian velocity distribution $f_b(v)dv$ is given by Eq. (22). Setting $t_0 = 0$ and using Eq. (32) we find

$$h_0(t) = f_b(L/t)L/t^2. \tag{33}$$

For analysis of our measurements this result has to be corrected for the v^{-1} dependence in the sensitivity of the quadrupole (see the section on calibration), yielding the effective TOF distribution $h(t) \sim f_b(L/t)/t$ written in a normalized form as

$$h(t) = f_s(L/t)L/t^2. \tag{34}$$

For our Maxwellian distribution, $f_s(x)$ is defined by Eq. (21) and we can write

$$h(t) = \frac{4}{\sqrt{\pi}}\frac{1}{\theta}\left(\frac{\theta}{t}\right)^4 e^{-(\theta/t)^2}, \tag{35}$$

where $\theta = L/\alpha$ is the TOF of the atoms with velocity α (see Fig. 7, curve 1). Thus, a very simple relation exists between the velocity distribution in the accommodator and the effective TOF distribution $h(t)$ as measured using a mass spectrometer.

The linearity of $\underline{\underline{T}}$ may be used to show that $S(t)$ can be written as a convolution integral:

$$S(t) = \int_{-\infty}^{t} e(\tau)h(t-\tau)d\tau \equiv e(t)*h(t). \tag{36}$$

A useful property of this integral involves the time de-

rivative:

$$\dot{S}(t) = \dot{e}(t) * h(t). \tag{37}$$

H. Narrow slit chopper

A common procedure to pulse atomic beams is to use fast rotating chopper blades containing one or more narrow slits. The finite width of any real beam or chopper can be accounted for using Eq. (36). Assuming a rectangular gate function (Fig. 7, curve 2′) the response of the detector is given by (Fig. 7, curve 2)

$$S(t) = S_0 \int_{t_0}^{t_1} h(t - \tau) d\tau, \tag{38}$$

where S_0 is the signal in absence of the chopper and the gate is assumed to be open between t_0 and t_1. High resolution requires the use of narrow slits; however, Eq. (38) shows that in the limit of a vanishing slit width ($t_1 - t_0 \rightarrow 0$), the signal also vanishes.

I. Equal segmented chopper

In our apparatus we employ an equal segmented chopper to obtain the TOF. Here the stimulus $e(t)$ is ideally represented by a step function $\theta(t - t_0)$ changing value at $t = t_0$

$$S(t) = S_0 \int_{-\infty}^{t} \theta(\tau - t_0) h(t - \tau) d\tau. \tag{39}$$

Knowing the response to the step function (Fig. 7, curve 3) the (effective) TOF distribution is obtained by differentiating $S(t)$ with respect to time:

$$\dot{S}(t) = S_0 h(t - t_0). \tag{40}$$

As in the case of the narrow slit chopper, one has to account for the finite width of any real beam. This results in a distortion of the step function which, however, remains simple if slit shaped diaphragms are used to define the beam (Fig. 7, curve 4′):

$$e(t) \equiv \begin{cases} 0 & \text{for} \quad t < t_0 \\ \dfrac{t - t_0}{t_1 - t_0} & \text{for} \quad t_0 < t < t_1 \\ 1 & \text{for} \quad t < t_1 \,. \end{cases} \tag{41}$$

The response to this $e(t)$ is calculated by substituting Eq. (41) into Eq. (36) and is plotted in Fig. 7, curve 4. The response is related to the TOF by applying Eq. (37)

$$\tilde{h}(t) \equiv \dot{S}(t) \frac{S_0}{t_1 - t_0} \int_{t_0}^{t_1} h(t - \tau) d\tau. \tag{42}$$

$\tilde{h}(t)$ is called the convoluted (effective) TOF distribution and is recognized as closely equivalent to the convolution of $h(t)$ with the rectangular gate function [i.e., Eq. (38)]. However, in contrast to that case, in the limit $t_1 \rightarrow t_0$, $\tilde{h}(t)$ reduces to $S_0 h(t - t_0)$ and high resolution may be obtained without any loss of signal. In comparing the merits of both techniques we must also include noise considerations. If one is completely limited by background noise, the equal segmented chopper will be favorable, whereas in the limit of vanishing background noise the narrow slit chopper will yield better results, since it minimizes noise due to fluctuations in the signal itself, such as those encountered for Poisson statistics. Except for the large background signal the possibility of simultaneously monitoring the total atomic flux by standard lock-in techniques was decisive for our choice. In the development of a cold H source, the beam flux is often unmeasurably small. Using a narrow slit chopper requires about 15 min of signal averaging to ascertain this, whereas about 1 s is required with lock-in detection, using an equal segmented chopper.

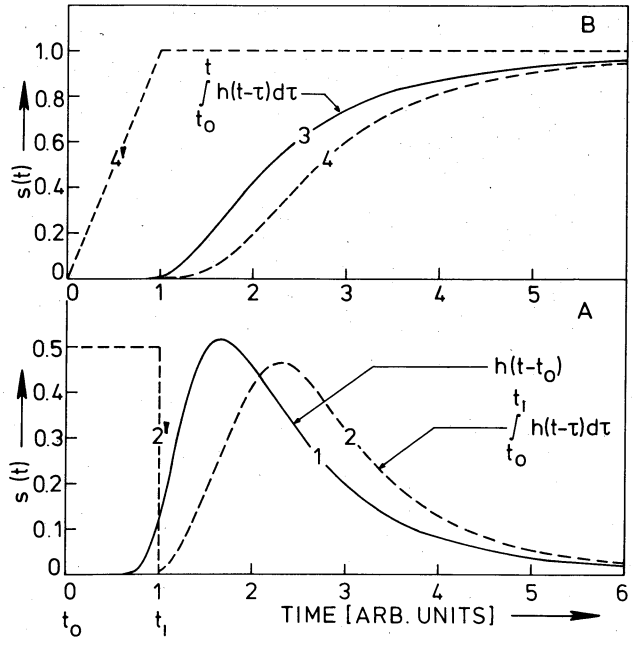

FIG. 7. TOF distributions for a Maxwellian beam and various choices of $e(t)$. (A) Case of narrow slit chopper. Curve 1: response to delta function stimulus. Curve 2: response to block pulse shown as curve 2′. (B) Case of equal segmented chopper. Curve 3: response to step function. Curve 4: response to step function, taking into account the finite cut-off time of the beam as shown with curve 4′. The areas under curves 1 and 2 are normalized to 1. Note that curves 1 and 2 are the derivatives of curve 3 and 4, respectively.

J. Signal processing

The signal originating from the mass spectrometer was averaged on a Fabri-Tek waveform analyzer using 256 channels and a 20-s dwell time. Typically, averaging was done over 10^5 spectra. The repetition rate is limited by the width of the TOF spectrum, too high a rate causing overlap of spectra and resulting in a distortion of the low-velocity part of the distribution. No special arrangements, such as the use of a double bladed chopper,[48,49] were undertaken to remove this low-velocity tail. The data was transmitted to a PDP 11 mini computer where further signal processing was done. $\tilde{h}(t)$ was obtained by numerical differentiation of $S(t)$ with respect to time using the Lanczos method.[50] Then, applying Eq. (34) the data (transformed to the velocity domain) yielded the convoluted (effective) velocity distribution $\tilde{f}_s(v)$. Finally

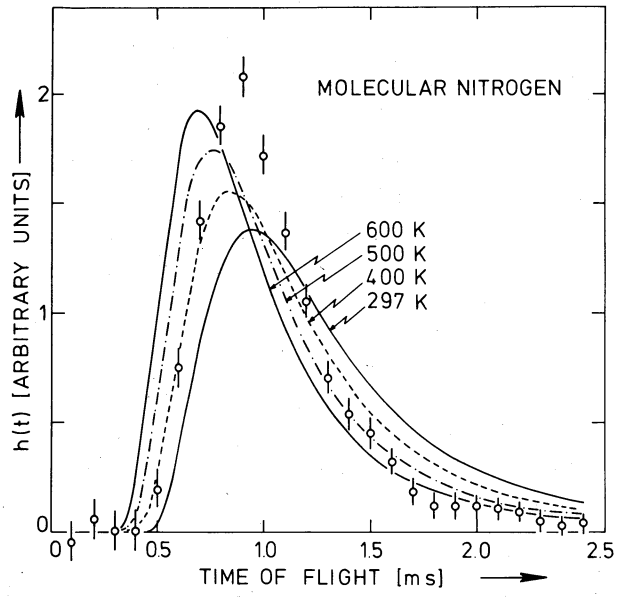

FIG. 8. Non-Maxwellian TOF distribution as measured in our system for molecular nitrogen at room temperature. For explanation, see text.

the data was smoothed using a Gaussian smoothing procedure, where the width of the Gaussian $(2/\sqrt{\lambda})$ was 25 m/s:

$$\langle \tilde{f}_s(v) \rangle = \int_{-\infty}^{+\infty} e^{-\lambda(v-\nu)^2} \tilde{f}_s(\nu) d\nu. \tag{43}$$

For high velocities ($v \gtrsim 2$ km/s) the width was taken slightly larger in order to prevent the corresponding width in the time domain from becoming less than the experimental resolution (0.13 ms).

Any smoothing results in deformation of the signal, most apparent in regions of large curvature. This effect is minimized by first subtracting a theoretical curve $\tilde{f}_s^{\text{th}}(v)$ selected by trial and error to approximately fit the data, and then to do the smoothing on the noisy difference signal, where significant deviations from the trial distribution must have a small second derivative. Then, after smoothing, the difference signal is added again to $\tilde{f}_s^{\text{th}}(v)$ to produce the (smoothed) total signal:

$$\langle \tilde{f}_s(v) \rangle = \tilde{f}_s^{\text{th}}(v) + \int_{-\infty}^{+\infty} e^{-\lambda(v-\nu)^2} [\tilde{f}_s(v) - \tilde{f}_s^{\text{th}}(\nu)] d\nu. \tag{44}$$

The advantage of this method is that deformation due to smoothing can only occur in the relatively small difference signal, which in our case is the deviation from ideal Maxwell–Boltzmann behavior. The approach is especially useful in measurements where the exact shape of the distribution is not too critical, such as in the present experiment where the TOF is used to determine the (Maxwellian) temperature of an ensemble of H atoms in a cryogenic environment.

K. Calibration of the time-of-flight scale

The signal averager was triggered using a pulse generated by an optical chopping indicator. There is, however, a phase difference between the real chopping function of the beam and the periodic trigger signal resulting from the electronics of the chopping indicator. Basically this phase difference originates from the difference in position between the beam and the chopper indicator, but is also due to the ion extraction time, the finite width of the trigger pulse, and the pulse handling electronics. Evidently the measurement time scale, i.e., the time initiated by the trigger pulse, has to be corrected in order to obtain the real experimental time scale. David *et al.*,[51] determined this zero of flight time by variation of the flight path. Miller[52] used UV photons and an on axis ion detector. A mechanical velocity selector was used by Beyerinck *et al.*,[49] to produce a known velocity beam, they also replaced the molecular beam by a light source using a photomultiplier for detection. Not all authors specify the estimated error in the zero of time determination but it seems difficult to achieve a high absolute accuracy since uncertainties up to 50 μs are reported. Clearly this calibration requires great care because of the many aspects that come into play. We used two independent methods to calibrate the time scale of our TOF system. First, an optical technique was used, replacing the beam by a small He–Ne laser and detecting the light using a fast light powermeter. This measurement yielded a shift corresponding to 210 ± 20 μs. This figure has to be corrected for the time delay due to the finite ion-extraction time when using an atomic beam instead of light. Such a correction is mass dependent and for H and H_2 calculated to be of the order of 4.1 ± 1 and 5.8 ± 1 μs, respectively. The second method used to calibrate the TOF time scale is based on the assumption that our source, operated at low enough pressures, will yield a Maxwellian velocity distribution. Then a simple fitting procedure with a calculated distribution can be used to fix the time scale. This procedure was used with H, H_2, and ^{4}He at room temperature and leads to a phase correction of 240 ± 5 μs. We also measured the distributions of Ne, N_2, and Ar but in these cases the pressures could not be reduced enough to observe Maxwell–Boltzmann behavior, due to noise limitations. In Fig. 8 the TOF distribution of N_2 at 295 K is plotted and compared with MB curves calculated for four different temperatures, taking into account convolution effects due to the slit function. The curves are normalized to the integrated intensity under the measured TOF distribution. The observed deviations from the 295 K MB curve cannot be eliminated by a shift in the time scale, demonstrating that knowledge of the beam temperature is sufficient to distinguish a Maxwellian from a non-Maxwellian distribution and giving confidence that the observed (Maxwellian) TOF distributions of H, H_2, and ^{4}He can be used to obtain a reliable time scale calibration.

No satisfactory explanation was found for the 25-μs discrepancy between the two calibration techniques. A number of instrumental effects that can induce a systematic error consistent with the observed discrepancy will be briefly discussed here. The 0.13 ms cut-off time of the beam gives rise to an important convolution correction especially for low-mass, high-temperature beams (Fig.

9). A possible systematic error might be due to incomplete knowledge of the instrumental function used in the convolution. This function was calculated assuming an ideal rectangular cross section of the beam and a position independent detection probability. The ionizer of a mass quadrupole will induce a distortion of the TOF spectrum if it is operated above a critical emission current due to the buildup of space charge causing ion-extraction problems. No changes in the TOF spectrum were observed by variation of the emission current up to 1.9 mA. Finally, memory effects may be present due to periodic fluctuations of the background pressure at the detection frequency caused by the beam randomized in the detection chamber. This effect is small in our system. The beam is passed through the open structured ionizer of the quadrupole and well collimated, so that beam particles will not collide with the walls of the ionizer. Furthermore, the final beam is randomized in a large volume (100 l) and pumped using a ion-getter/titanium sublimation pumping combination with an overall pumping speed of 6000 l/s for hydrogen. For average beam velocities below 500 m/s, of primary concern in studying low-temperature beams, uncertainties of order 25 μs in the TOF time scale correspond to errors of less than 2.5% in the velocity or 5% in the Maxwellian temperature. The TOF system parameters are summarized in Table I.

III. RESULTS

As a typical example of the results that can be achieved with our dissociator design we first discuss a measurement of α that was done with the tube shown in Fig. 3b. Here, the H leaving the discharge enters into a $L = 90$ mm, $r = 2$ mm [$\bar{N}_c \simeq 759$, see Eq. (7a)] quartz tube cooled to liquid nitrogen temperature. We measured $\alpha \simeq 0.92 \pm 0.02$ for an estimated flux $\phi_{in} \simeq 2 \times 10^{18}$/s. Analyzing this result on the basis of first-order recombination kinetics [$\alpha \simeq 1 - \gamma\bar{N}_c$; for $\gamma\bar{N}_c \ll 1$, see Eq. (1b)]. We calculate $\gamma \lesssim 10^{-4}$. This result represents an upper limit since we assumed implicitly that ϕ_{in} is fully dissociated. Moreover, experience with other tubes leads to the conclusion that the gas leaving the discharge region is never more than 94% dissociated.

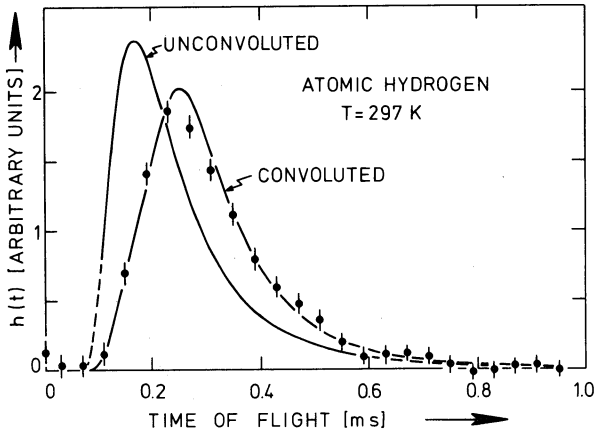

FIG. 9. The importance of convolution for fast beams demonstrated for the TOF of atomic hydrogen at room temperature.

TABLE I. TOF system parameters.

flight distance	525 ± 5 mm
beam diameter at chopper	1.5 ± 0.02 mm
angular velocity of chopper	177.5 ± 1 rad/s
chopping period	8.85 ± 0.05 ms
resolution of signal averager	20 μs
time resolution (cut-off time)	0.130 ± 0.002 ms

The most complete set of results was obtained with the apparatus shown in Figs. 1, 2, 3a, and 6 discussed in detail in Sec. I. We stabilized the total mass flow through the system using the precision needle valve and selected a relatively low flow rate to ensure the absence of interference between beam and background gas. At room temperature we measured $\phi_H = 7.2 \times 10^{16}$/s with $\alpha \simeq 0.31$. The Teflon tube connecting dissociator with accommodator is characterized by $\bar{N}_c \simeq 3750$ [using Eq. (7a)]. Equation (9b) now enables an estimate of γ_{Teflon}, yielding $\gamma_{Teflon} \simeq 4.5 \times 10^{-4}$. Under the best conditions we observed $\gamma_{Teflon} \simeq 10^{-4}$ for commercial Teflon tubing. No attempts were made to study the recombination kinetics. Reducing the accommodator temperature to 78 K, the H flux decreased to 65% of the room temperature value. Further cooling to 7.7 K (the lowest achievable temperature for the accommodator) resulted in a flux decrease to 32% or $\phi_H \simeq 2.4 \times 10^{16}$ H_1/s. On the basis of these results we calculate average densities of 3.4×10^{13}/cm^3 at $T = 7.7$ K in the accommodator [using Eq. (28)]. Once the temperature of the accommodator is reduced, a detailed comparison between experiment and the model presented in Sec. I is no longer justified due to the presence of temperature gradients. Especially at the lowest temperatures, care is required in interpreting our results in view of uncertainties in the peaking correction for the beam, which is hard to estimate but could be on the order of a factor of 1.5. However, it is most likely that the reduction in atomic flux—with lowering of the accommodator temperature—is due to an increase in the recombination probability γ. If we assume this point of view we must conclude that the surface of the accommodator is not covered with a saturated layer of solid molecular hydrogen. Using the results of Crampton[35] we calculate $\gamma = 5 \times 10^{-6}$ at 8 K and $n = 10^{14}$/cm^3. For our accommodator $\bar{N} \simeq 38$, implying that recombination would be negligible. A thick film of H_2 is also inconsistent with our H_2 intensity measurements. A saturated vapor pressure would result in a H_2 beam three orders of magnitude more intense than was observed experimentally. The exact composition of the accommodator surface is unknown, although it seems reasonable to assume a surface coverage of, at most, a few monolayers of solid H_2.

Evidence that the gas was well accommodated to low temperature was obtained by measuring the TOF distribution at the various accommodator temperatures. The raw data, an example of which is shown in Fig. 10, was reduced to velocity distributions using the formalism of Sec. II. Results are shown in Fig. 11(a) for the three different measured temperatures: 297 ± 3, 78 ± 2, and 7.7 ± 1 K. The difference in error bar for different ve-

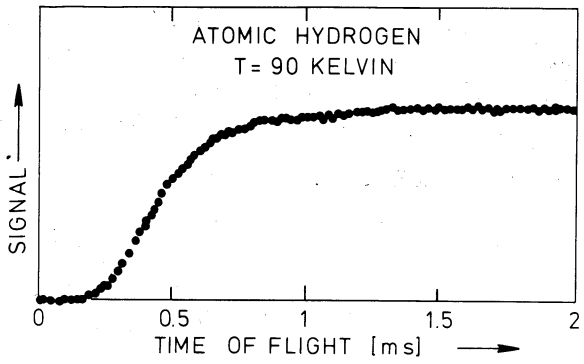

FIG. 10. An example of raw data as obtained for atomic hydrogen at $T = 90$ K.

locities results from the transformation from time to velocity space: the TOF can be measured very accurately for a low-velocity beam due to a large dispersion in time, however this dispersion also leads to low intensities and thus relatively large vertical error bars. The data can be fit to Maxwellian distributions (convoluted with the slit function) corresponding to temperatures 297 ± 5, 90 ± 5, and 8.5 ± 1 K. These temperatures were found to be consistent with the distributions measured for H_2 [see Fig. 11(b)] with discharge on. On the basis of the 8.5 K TOF we calculate an increase in the flux of low-velocity atoms ($v < 2v_\beta = 918$ m/s, where v_β is the most probable velocity in the beam) by a factor $\simeq 20$ with respect to the room-temperature beam. (The reduction from the theoretical maximum value of 71 is due to increased recombination losses.) This result shows that our source, in combination with a velocity selector, could be a valuable tool for low-energy atomic beam scattering experiments with hydrogen atoms.

It is useful to raise the question of what is to be expected if the accommodator is operated at still lower temperatures—say below 4 K. We expect a steadily growing layer of solid molecular hydrogen to form; the calculated output flux of H_2—based on the known vapor pressure of the solid[53]—is much smaller than typical input fluxes. We thus may base our analysis on the work of Crampton,[35] using an exponential scaling of the recombination rate with temperature $K_{S2} = K_{S2}{}^0 T^{-1/2} \exp(2\epsilon_a/kT)$.[34] Recombination rapidly becomes limiting once $\bar{N}_c \gtrsim 1/\gamma = \bar{v}/(4K_{S2}n)$. Replacing n by the average density in the accommodator and using expressions (7a) and (28) we obtain a simple criterion to decide whether the flux is recombination limited or not

$$\phi_H \gtrsim \left(\frac{64}{9}\right)\left(\frac{r^5}{l^3}\right)\left(\frac{kT^{3/2}}{m_H}\right)\left(\frac{1}{K_{S2}{}^0}\right)\left[\exp\left(\frac{-2\epsilon_a}{kT}\right)\right],$$

where r, l, and T are the radius, length, and temperature of the accommodator, respectively, $\epsilon_a = 38$ K and $K_{S2}{}^0 = 8.4 \times 10^{-20}$ cm^4 K$^{1/2}$ s^{-1}.[54] With this expression, recombination is found to become limiting for our accommodator at 4 K if $\phi_H \gtrsim 10^{16}$/s. However, the effect has a strong temperature dependence. At 2.5 K we expect to be recombination limited already for $\phi_H \gtrsim 10^{11}$/s. Of course, one may try a brute force approach of using high input fluxes and accept considerable recombination losses to obtain some increase in output flux. We note that this approach is very inefficient since recombination on H_2 is second order and, therefore, scales with $\bar{n}^2$. To double ϕ_H (roughly proportional to $\bar{n}$) we thus have to quadruple the input flux into the accommodator so that, even with $\phi_{in} = 10^{17}$/s one only obtains $\phi_H \simeq 10^{14}$/s at 2.5 K. Additional disadvantages of the brute force approach are the considerable heat load and the rapid buildup of bulk solid which may give rise to plugging up of the accommodator. A recombining flux $\phi_H = 10^{17}$/s corresponds to 7 mm^3 bulk solid per hour and a recombination heat load of 36 mW.

A simple method to increase the recombination limited flux by approximately one order of magnitude would be to reduce the length of the accommodator by a factor of 2. This would of course reduce the number of wall collisions to below 10 but the masses of H and H_2 are well enough matched to enable efficient energy accommodation in a few collisions, so that the beam temperature would remain unchanged.

A serious problem which can exist is a vacuum leak of air into the Teflon tube. In one such case after cooling we observed the flux of H to deteriorate from a high value to zero within some tens of minutes. Presumably the air condenses on the cold Teflon surfaces before the accommodator and these air surfaces, which are not covered with H_2, are efficient for recombination. We believe that the most important process is first-order recombination of H with oxygen. Precautions should always be taken to use pure H_2 gas and to protect the Teflon from condensable gases or oils.

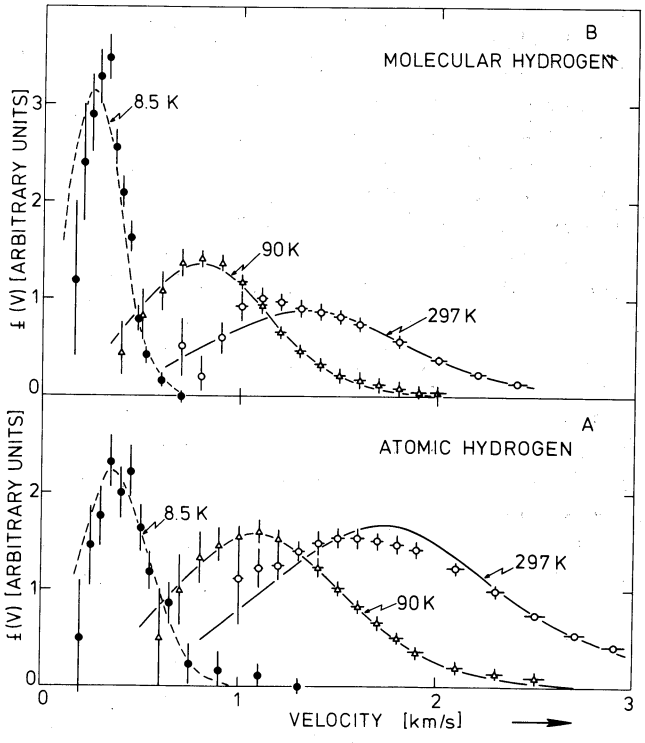

FIG. 11. The velocity distribution of atomic and molecular hydrogen as measured for three different temperatures.

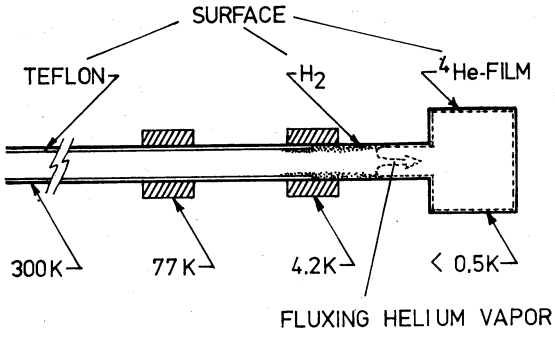

FIG. 12. Schematic diagram of the experimental arrangement of Ref. 4 to load H into a cell with helium covered walls at temperatures below 0.5 K.

Subsequent to the measurements reported here, sources based on these designs, operated at an accommodator temperature of $T = 4$–6 K were used to load H into cells with liquid helium covered walls at temperatures below ~0.5 K (see Fig. 12 and Ref. 4). An important design consideration of these sources has been to avoid collisions of H with non-helium covered surfaces below 4.2 K. This was realized by using a very short tube between the accommodator and the helium covered region, thus tolerating incomplete accommodation on the H_2 surface to avoid total recombination. A nonquantitative confirmation of the importance of the accommodator wall temperature was found when deuterium was loaded into a similar helium covered cell.[55] In this case the flux was orders of magnitude lower than when loading with H under similar conditions, due to the larger adsorption energy of D on D_2 (this is unmeasured but must be larger due to the lower zero-point energy). Moderate heating of the accommodator yielded substantial gains in flux.

An additional complication of configurations employing superfluid helium covered surfaces at low temperature may be the presence of stagnant helium gas in the accommodator and transport tube. If the mean-free-path λ of the H atoms in the stagnant gas is smaller than the diameter of the tube, the transport of the H is no longer Knudsen limited but may be described by ordinary diffusion (with $D = \frac{1}{3}\lambda\bar{v}$). This leaves the analysis of Sec. I unchanged if we correct for an enhanced number of wall collisions in the accommodator and transport tube: $\bar{N}_c^{\text{diff}} = \bar{N}_c(2r/\lambda)$. For a pressure $p = 10^{-2}$ Torr (corresponding to the saturated vapor pressure of ^{4}He at 0.8 K), the density of the stagnant gas in the accommodator (assumed to be at 4 K) is $n \simeq 3 \times 10^{16}/\text{cm}^3$, corresponding to $2r/\lambda \simeq 50$ or equivalently a reduction of ϕ_H by the same amount if the flux is recombination limited.

Further, we note that the most perilous region for the H atoms is that between the 4 K accommodator and the ~0.5 K cell. Between these two regions of the tube the helium film is driven towards the accommodator and vaporizes at a point, where $T \lesssim 1$ K, fluxing back to the cold region.

In the region 1–4 K, the H_2 wall may be covered by only a monolayer or so of helium and we expect most H atoms that strike those walls to recombine. Obviously this region should be made as short as possible so that atoms can make the transition without wall collisions. A stagnant He gas can possibly frustrate this. Alternatively much "hotter" atoms can be fluxed through this region.

ACKNOWLEDGMENTS

The authors thank E. Hartman for assistance with the data handling, O. H. Höpfner for his technical support and A. Zwart for making the dissociator tubes. We gratefully acknowledge the financial support of the Stichting FOM.

[1] S. B. Crampton, T. J. Greytak, D. Kleppner, W. D. Phillips, D. A. Smith, and A. Weinrib, Phys. Rev. Lett. **42,** 1039 (1979).
[2] W. N. Hardy, A. J. Berlinsky, and L. A. Whitehead, Phys. Rev. Lett. **42,** 1042 (1979).
[3] I. F. Silvera and J. T. M. Walraven, Phys. Rev. Lett. **74A,** 193 (1979).
[4] I. F. Silvera and J. T. M. Walraven, Phys. Rev. Lett. **44,** 164 (1980).
[5] S. B. Crampton, W. D. Phillips, D. Kleppner, Bull. Am. Phys. Soc. **23,** 86 (1978).
[6] M. Morrow, R. Jochemsen, A. J. Berlinsky, and W. N. Hardy, Phys. Rev. Lett. **46,** 195 (1981); **47,** 455 (1981).
[7] W. Welz, thesis, Bonn, 1976, Max-Planck-Institut für Strömungsforschung, Göttingen, Bericht 20/1976 (unpublished); see also J. P. Toennies, W. Welz and G. Wolf, J. Chem. Phys. **71,** 614 (1979).
[8] M. Perrenoud, W. Grüebler, and V. König, Helv. Phys. Acta **44,** 594 (1971).
[9] A. A. Belushkina, V. P. Vadeev, A. I. Valevich, G. I. Goi, E. D. Donets, V. P. Ershov, L. S. Kotova, Y. A. Plis, Y. K. Pilipenko, and V. V. Smelyanskii, Instrum. Exp. Tech. (U.S.A.) **19,** 1618 (1976).
[10] Y. Wakuta, Y. Koga, H. Hasuyama, and H. Yamamoto, Nucl. Instrum. Methods **147,** 461 (1977).
[11] L. Dick and T. Niinikoski; G. Clausnitzer (private communications).
[12] *Formation and Trapping of Free Radicals*, edited by A. M. Bass and H. P. Broida (Academic, New York, 1960).
[13] R. Hess, thesis, Stuttgart, 1971.
[14] Our system is similar to the dissociator described by G. O. Brink, R. O. Fluge, and R. J. Hull, Rev. Sci. Instrum. **39,** 1171 (1968). Other designs are discussed in F. C. Fehsenfeld, K. M. Evenson, and H. P. Broida, Rev. Sci. Instrum. **36,** 294 (1965); B. McCarroll, Rev. Sci. Instrum. **41,** 279 (1970); A. Ding, J. Karlau, and J. Weise, Rev. Sci. Instrum. **48,** 1002 (1977); D. Walker, R. M. St. John, J. Chem. Phys. **61,** 2394 (1974); K. R. Way, Sze-Cheng Yang, and W. C. Stwalley, Rev. Sci. Instrum. **47,** 1049 (1976); see also Ref. 7.
[15] *Very High Frequency Techniques*, Vol. II, edited by H. J. Reich (McGraw-Hill, New York, 1947).
[16] V. H. Ritz, V. M. Bermudez, and V. J. Folen, J. Appl. Phys. **48,** 2096 (1977).
[17] P. L. Chambré, J. Chem. **32,** 24 (1960).
[18] A. T. Lifshits, I. M. Metter, and L. E. Rikenglaz, Sov. Phys. Tech. Phys. **16,** 276 (1971).
[19] H. Wise and B. J. Wood, in *Advances in Atomic and Molecular Physics*, Vol. 3, edited by D. R. Bates and I. Estermann (Academic, New York, 1967) pp. 291–353.
[20] We note that except for the factor A/V, K_{S2} equals K_S^{eff} used in Ref. 34.
[21] D. N. Mitchell and D. J. Le Roy, J. Chem. Phys. **67,** 1042 (1977).
[22] M. Knudsen, Ann. Physik (Leipzig) **28,** 999 (1909).
[23] P. Clausing, Z. Phys. **66,** 593 (1930); P. Clausing, thesis, Leiden, 1928.
[24] S. Dushman, in *Scientific Foundations of Vacuum Technique*, 2nd ed., edited by J. M. Lafferty (Wiley, New York, 1962), p. 93.
[25] As the cross sections are different for singlet and triplet collisions here we used an average, the viscosity cross section, $\sigma = 55$ Å^2 at $T = 300$ K as calculated by R. A. Buckingham and E. Gal, Adv. At. Mol. Phys. **4,** 37 (1968).
[26] J. E. Bennet and D. R. Blackmore, Proc. R. Soc. London, Ser. A **305,** 553 (1968).
[27] A. Salop and A. Mandl, J. Phys. E **4,** 645 (1971).
[28] A. Mandl and A. Salop, J. Appl. Phys. **44,** 4776 (1973).
[29] M. Coulon, J. C. Fanton, and L. Bonnetain, J. Chim. Phys. **70,** 1493 (1973).

[30] Edited by M. Abramowitz and I. A. Stegun, *Handbook of Mathematical Functions*, National Bureau of Standards Applied Mathematics Series no. 55, U.S. Government Printing Office, Washington, D.C. (1964).
[31] See Ref. 30 relations 18.13.67 and 18.13.68.
[32] We use $\sigma = 1.6 \times 10^{-16}$ cm^2, where $\sigma = 4\pi a^2$ and $a = 0.72$ Å is the s-wave scattering length as calculated for the triplet potential by D. G. Friend and R. D. Etters, J. Low. Temp. Phys. **39,** 409 (1980).
[33] W. N. Hardy, M. Morrow, R. Jochemsen, B. W. Statt, P. R. Kubik, R. M. Marsolais, A. J. Berlinsky, and A. Landesman, Phys. Rev. Lett. **45,** 453 (1980).
[34] A. P. M. Matthey, J. T. M. Walraven, and I. F. Silvera, Phys. Rev. Lett. **46,** 668 (1981).
[35] S. B. Crampton, J. Phys. (Paris) **41,** C7-249 (1980); see also S. B. Crampton, T. J. Greytak, D. Kleppner, W. D. Phillips, D. A. Smith, and A. Weinrib, Phys. Rev. Lett. **42,** 1039 (1979).
[36] G. H. van Yperen, A. P. M. Matthey, J. T. M. Walraven, and I. F. Silvera, Phys. Rev. Lett. **47,** 800 (1981).
[37] R. Jochemsen, M. Morrow, A. J. Berlinsky, and W. N. Hardy, Phys. Rev. Lett. **47,** 852 (1981).
[38] H. Wilsch, J. Chem. Phys. **56,** 1412 (1971).
[39] Du Pont de Nemours & Co. The use of this dispersion was pointed out to us by W. D. Phillips.
[40] J. A. Giordmaine and T. C. Wang, J. Appl. Phys. **31,** 463 (1960).
[41] V. S. Troitskii, Sov. Phys. Tech. Phys. **7,** 353 (1962).
[42] D. R. Olander and V. Kruger, J. Appl. Phys. **41,** 2769 (1970).
[43] N. F. Ramsey *Molecular Beams* (Clarendon, Oxford, 1956).
[44] D. R. Olander, R. H. Jones, and W. J. Siekhaus, J. Appl. Phys. **41,** 4388 (1970).
[45] E. H. Kennard *Kinetic Theory of Gases* (McGraw-Hill, New York, 1938).
[46] W. J. Siekhaus, R. H. Jones, and D. R. Olander, J. Appl. Phys. **41,** 4392 (1970).
[47] R. G. Wilmoth, J. Vac. Sci. Technol. **9,** 1121 (1972).
[48] H. C. W. Beyerinck, and N. F. Verster, J. Appl. Phys. **46,** 2083 (1975); H. C. W. Beyerinck, thesis, Eindhoven, The Netherlands, 1975.
[49] H. C. W. Beyerinck, R. G. J. M. Moonen, and N. F. Verster, J. Phys. E. **7,** 31 (1974).
[50] C. Lanczos, *Applied Analysis*, Pitman, London, 1957.
[51] R. David, M. Faubel and J. P. Toennies, Chem. Phys. Lett. **18,** 87 (1973).
[52] T. M. Miller, J. Appl. Phys. **45,** 1713 (1974).
[53] B. N. Esel'son, Y. P. Blagoi, V. N. Grigor'ev, V. G. Manzhelli, S. A. Mikhailenco, and N. P. Neklyndov, *Properties of Liquid and Solid Hydrogen*, (Keter Press, Jerusalem, 1971).
[54] This value was derived from the results of Crampton, see Ref. 35.
[55] I. F. Silvera and J. T. M. Walraven, Phys. Rev. Lett. **45,** 1268 (1980).